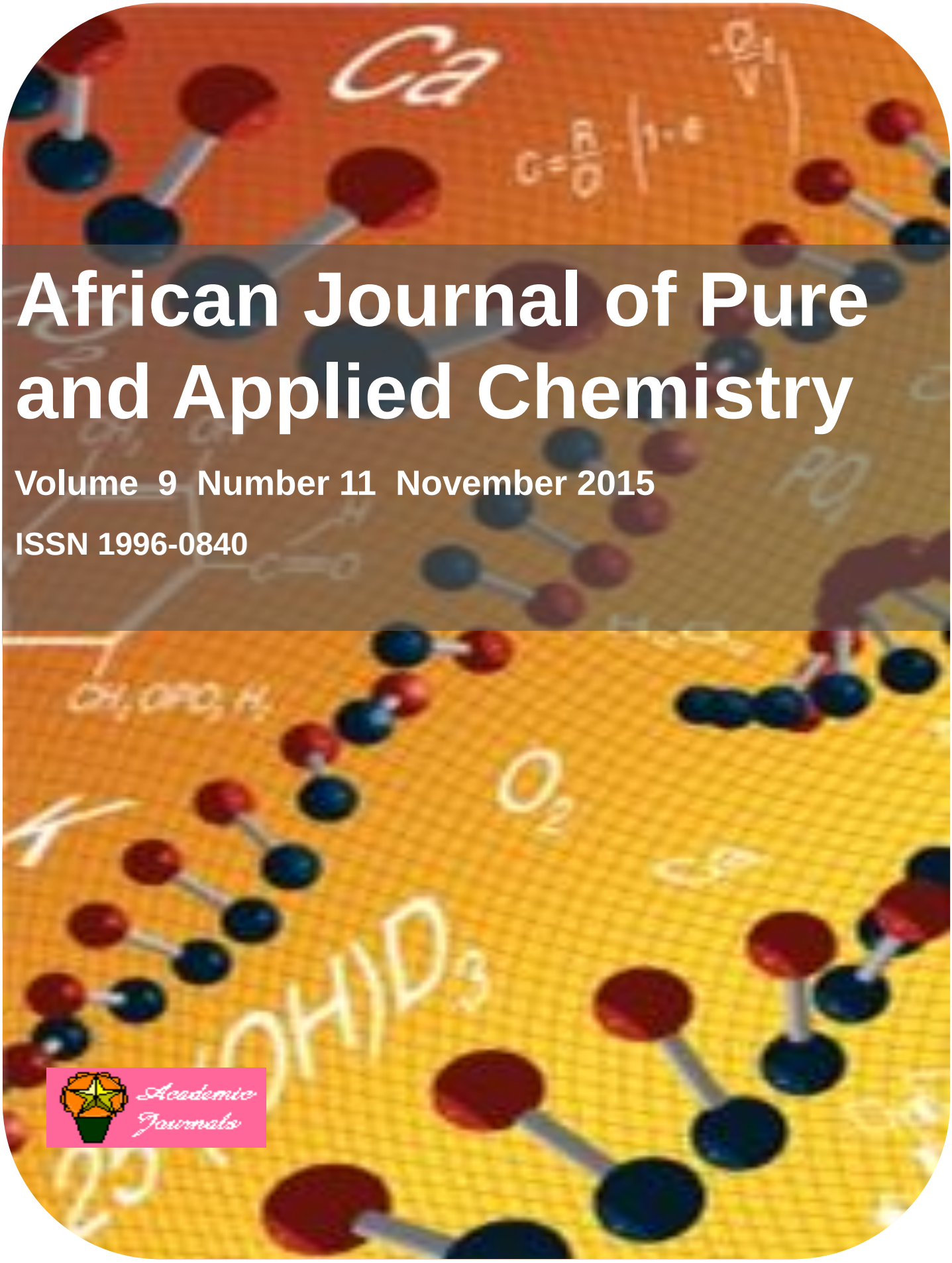

African Journal of Pure and Applied Chemistry

Volume 9 Number 11 November 2015

ISSN 1996-0840

Academic Journals

ABOUT AJPAC

The **African Journal of Pure and Applied Chemistry (AJPAC)** is an open access journal that publishes research analysis and inquiry into issues of importance to the science community. Articles in AJPAC examine emerging trends and concerns in the areas of theoretical chemistry (quantum chemistry), supramolecular and macromolecular chemistry, relationships between chemistry and environment, and chemicals and medicine, organometallic compounds and complexes, chemical synthesis and properties, chemicals and biological matters, polymer synthesis and properties, nanomaterials and nanosystems, electrochemistry and biosensors, chemistry and industry, chemistry and biomaterials, advances in chemical analysis, instrumentation, speciation, bioavailability. The goal of AJPAC is to broaden the knowledge of scientists and academicians by promoting free access and provide valuable insight to chemistry-related information, research and ideas. AJPAC is a bimonthly publication and all articles are peer-reviewed.

African Journal of Pure and Applied Chemistry (AJPAC) is published twice a month (one volume per year) by Academic Journals.

Contact Us

Editorial Office: ajpac@academicjournals.org

Help Desk: helpdesk@academicjournals.org

Website: http://www.academicjournals.org/journal/AJPAC

Submit manuscript online http://ms.academicjournals.me/.

Editors

Editorial Board

African Journal of Pure and Applied Chemistry

Table of Contents: Volume 9 Number 11 November 2015

ARTICLE

academicJournals

Vol. 9(11), pp. 204-210, November, 2015
DOI: 10.5897/AJPAC2015.0654
Article Number: 4392E4856200
ISSN 1996 - 0840

http://www.academicjournals.org/AJPAC

African Journal of Pure and Applied Chemistry

Review

Health risk assessment of heavy metals in water, air, soil and fish

Isa Baba Koki[1]*, Amina Salihi Bayero[1], Aminu Umar[1] and Sabo Yusuf[2]

[1]Department of Chemistry, Northwest University, P. M. B. 3220, Kano, Nigeria.
[2]Department of Chemistry, Bayero University, P. M. B. 3011, Kano, Nigeria.

Received 26 August, 2015; Accepted 22 October, 2015

The study and application of health risk assessment techniques are crucial in order to understand the risk of exposure to heavy metals and other harmful pollutants. It entails evaluating the risks of exposure at various concentrations and with reference to certain standard values approved by World Health Organization (WHO) and United States Environmental Protection Agency (USEPA). Investigation of water contamination with heavy metals has become the prime focus of environmental scientists in recent years. Effluent discharges into aquatic system affect living organisms within the receiving environment. The concentrations of these metals were mostly assessed at 50th, 75th and 95th percentile and various exposure evaluated. This review covers studies in water, air, soil and fish samples. Air risks assessment was not given the needed attention and children were more susceptible to the hazard than adult, especially lead toxicity, resulting in health complications. Heavy metals bio accumulates over time, and lethal upon exposure at low concentrations. This review will assist risk managers to minimize the exposure at optimum level as well as for the government to formulate policies in safe guarding the health of population.

Key words: Health risk assessment, pollution, heavy metals, water, air, soil.

INTRODUCTION

Water is an essential component of life, fresh water constitute about 3% of the total water on the earth surface, only 0.01% of this fresh water is available (Hinrichsen and Tacio, 2002), with two thirds of the earth's surface covered by water and the human body consisting of 75% of it, it is evidently clear that water is one of the prime elements responsible for life on earth. Regrettably, even this small portion of fresh water is under pressure due to anthropogenic sources due to rapid growth in population and industrial activities (Li et al., 2009). Heavy metals are the main pollutants and elements of risk in drinking water (Enaam, 2013).

Investigation on water contamination by heavy metals has become the prime focus of environmental scientists

*Corresponding author. E-mail: isakoki@yahoo.com.

in recent years (Fenglian and Qi, 2011). More attention should be given to toxic heavy elements because of bio accumulation and bio magnification potential, and their persistence in the environment. Some metals like copper (Cu), cobalt (Co) and zinc (Zn) are essential for normal body growth and functions of living organisms and are referred to as essential elements. Other elements are referred to as non-essential, high concentrations of these metals like cadmium (Cd), chromium (Cr), manganese (Mn), and lead (Pb) are considered highly toxic to human and aquatic life (Ouyang et al., 2002). A certain amount of Cr for instance is needed for normal body functions; but at the same time high concentrations may cause toxic effect such as liver, kidney problems and genotoxic carcinogen (Knight et al., 1997). Like Cr, Co is also one of the required metals needed for normal body functions as a metal component of vitamin B12 (Strachan, 2010). However, high intake of Co via consumption of contaminated food and water can cause abnormal thyroid artery, polycythemia, over-production of red blood cells (RBCs) and right coronary artery problems (Robert and Mari, 2003).

Generally, high concentrations of Mn and Cu in drinking water can cause mental diseases such as Alzheimer's and Manganism (Dieter et al., 2005). High Mn contamination in drinking water also affects the intellectual functions of 10-year-old children (Wasserman et al., 2006). Similarly, the Ni-sulfate and Ni-chloride ingestion can cause severe health problems, including fatal cardiac arrest (Knight et al., 1997). Pb is also a highly toxic and carcinogenic metal and may cause chronic health risks, including headache, irritability, abdominal pain, nerve damages, kidney damage, blood pressure, lung cancer, stomach cancer and gliomas. As the children are most susceptible to Pb toxicity, their exposure to high levels of Pb cause severe health complexities such as behavioral disturbances, memory deterioration and reduced ability to understand, while long-term Pb exposure may lead to anemia (Jarup, 2003).

Like other heavy metals, sufficient amount of Zn is also very significant for normal body functions. Its deficiency can lead to poor wound healing, reduced work capacity of respiratory muscles, immune dysfunction, anorexia, diarrhea, hair loss (Strachan, 2010). Cd exposure can cause both chronic and acute health effects in living organisms (Barbee and Prince, 1999). The chronic effects includes kidney damage, skeletal damage and itai-itai (ouch-ouch) diseases (Jarup et al., 2000). Experimental data in humans and animals showed that Cd may cause cancer in humans, diarrhea, hair loss, dermatitis (Acrodermatitis enteropathica) and depression. Cd exposure can cause both chronic and acute health effects in living organisms (Barbee and Prince, 1999). The chronic effects includes kidney damage, skeletal damage and itai-itai (ouch-ouch) diseases (Jarup et al., 2000; Nordberg et al., 2002). Experimental data in humans and animals showed that Cd may cause cancer in humans (IARC, 1993).

HUMAN HEALTH RISK ASSESSMENT

Human health risk assessment is considered as the characterization of the potential adverse health effects of humans as a result of exposures to environmental hazards (USEPA, 2012). This process employs the tools of science, engineering, and statistics to identify and measure a hazard, determine possible routes of exposure, and finally use that information to calculate a numerical value to represent the potential risk (Lushenko, 2010). A human health risk assessment involves four steps which are: hazard identification, dose-response assessment, exposure assessment, and risk characterization. Health risk assessment classifies elements as, carcinogenic or non-carcinogenic. The classification determines the procedure to be followed when potential risks are calculated. Non-carcinogenic chemicals are assumed to have a threshold; a dose below which no adverse health effects will be observed where an essential part of the dose-response portion of a risk assessment includes the use of a reference dose (RfD). Also, carcinogens are assumed to have no effective threshold. This assumption implies that there is a risk of cancer developing with exposures at low doses and, therefore, there is no safe threshold for exposure to carcinogenic chemicals. Carcinogens are expressed by their Cancer Potency Factor (Lushenko, 2010).

EXPOSURE ASSESSMENT

The daily environmental exposures to metals were assessed for carcinogenic and non-carcinogenic elements. There are two main exposure pathways: intake of the metals through water consumption, and by skin absorption through bathing. Calculations were done based on USEPA standards (The United States Environmental Protection Agency (USEPA), 1996). Assessment of non-carcinogenic risks can be achieved by estimating the hazard quotient (HQ). it is calculated as the quotient between the environmental exposure and the reference dose (RfD). HQ values were obtained for each element and exposure pathway. Subsequently, the hazard index (HI), which is defined as the total risk through heath exposure pathway, was obtained by summing the HQ of each element. Finally, the total HI was calculated by summing the HI through oral and dermal routes (HIing and HIderm, respectively) (USEPA, 1989). Values of HI under the unity are considered as safe (USEPA, 1989). The HQ is considered to be an estimate of the risk level (non-carcinogenic) due to

Table 1. Parameters used for estimating exposure assessment in Water (Liang et al., 2011; Wu et al., 2009; Liu et al., 2007).

Risk exposure factors	Values	Unit
Ingestion Rate (IR)	2.2	L/day
Exposure Frequency (EF)	360	Days/year
Exposure Duration (ED)	30	Years
Average Time (AT)	h/day	0.6
Average Body Weight (BW)	kg	70
Carcinogenic Potency Slope (CPS)	$\mu g g^{-1} day^{-1}$	Pb=0.009,Ni=1.7, Cd=0.6

pollutant exposure with respect to EDI (estimated daily intake) which is calculated from the following equation:

$$HQ = EDI/RfD \quad (1)$$

A summation of the hazard quotients for all chemicals to which an individual is exposed was used to calculate the hazard index (USEPA, 2011).

$$HI = HQ_A + HQ_B + \ldots\ldots\ldots\ldots + HQn \quad (2)$$

Where HI is the hazard index; HQ_A is the target hazard quotient for A intake; HQ_B is the target hazard quotient for B intake, and HQ_n is the target hazard quotient for n intake.

Carcinogenic risk was evaluated by target cancer risk (TR). The method for estimating TR was provided in USEPA Region III Risk-Based Concentration (USEPA, 2011).

$$TR = (MC \times IR \times 10^{-3} \times CPS \times EF \times ED)/(BW \times AT) \quad (3)$$

Where TR is the target cancer risk; MC is the metal concentration in the sample ($\mu g\ g^{-1}$); IR is the ingestion rate ($g\ day^{-1}$); CPS is the carcinogenic potency slope, ($mg/kg\ bw\ day^{-1}$); and ATc is the averaging time, carcinogens ($days\ year^{-1}$). The description and values of the parameters for exposure in water are shown in Table 1.

Another way to estimate Carcinogenic risks is by calculating the increase possibilityof an individual to develop cancer as a result of exposure to the potential carcinogen over a lifetime. The estimated daily intake of toxin is converted by slope factor which is averaged by direct exposure over a lifetime to the increased chances of an individual to develop cancer (USEPA, 1989).

$$Risk = ADI * SF \quad (4)$$

Risk is therefore a unit less of chances of an individual developing cancer when exposed over a lifetime and SF is the carcinogenicity slope factor (per mg/kg/day) and ADI is the acceptable daily intake. Risks values exceeding 1×10^{-4} are regarded as intolerable, risks less than 1×10^{-6} are not regarded to cause significant health effects, and risks lying between 1×10^{-4} and 1×10^{-6} are regarded generally as satisfactory range, but circumstances and condition of exposure determine the range of the value of the circumstance (Hu et al., 2012). Heavy metal evaluation Index (HEI) gives an overall quality of the water with respect to heavy metals (Edet and Offiong, 2002).

$$HEI = \sum \frac{Mc}{MAC} \quad (5)$$

Where Mc is the observed metal concentration and MAC is the maximum allowable concentration of the metal in the water guideline.

Analysis of exposures in samples

Several researches were carried out on human exposure to toxic metals and other pollutants through water, soil, fishes and other foods. Among the heavy metals analyzed in Langat River and Cempaka lake Malaysia, Cr had the HQ value greater than 1 for culture pond A and culture pond B, Langat River. While the HQ value for Pb ranged from 0.017 to 0.073 which were much lower than those measured in Tri states mining districts where the HQ ranged from 0.1 to 4.6 (Schmitt et al., 2006). In the study at Langat River and Cempaka Lake, Malaysia, although the observed values of HQ for Pb, Cd, Ni, Cu and Zn were lower than the safe standard of 1, but ΣHQ of these metals (HI) were higher than 1. The calculated HI ranged from 0.24 to 1.88 which indicates that 71% of stations are in the risk level while Bandar and Jugra were the only stations analyzed with HI values of less than 1.

In Pakistan, the calculated chronic daily intake (CDI) values for consumption of drinking water suggest that in Jijal-Dubair area, people have consumed surface water contaminated with heavy metals, the maximum CDI values were 0.10, 0.02, 0.62, 3.76, 0.21, 0.23, 0.12, and

1.09 µg/kg/day for Cd, Co, Cr, Cu, Mn, Ni, Pb and Zn, respectively. But in Jijal-Dubairarea, the consumed ground water had maximum CDI values of 0.03, 0.09, 0.98, 3.64, 0.25, 0.40, 0.15, and 78.93 µg/kg-day for Cd, Co, Cr, Cu, Mn, Ni, Pb and Zn, respectively. CDI indices for heavy metal in the study area were found in the order of Zn > Cu > Mn > Pb > Cr > Ni > Cd > Co (Said et al., 2011). In drinking water, the high CDI values of Zn, Mn and Pb may be attributed to the Pb–Zn sulfide mineralization, while that of Cr and Ni may have resulted from the mafic and ultramafic bed rocks hosting chromite deposits (Miller et al., 1991; Ashraf and Hussian, 1982).

In a study carried out in northwestern Bangladesh, the proposed HEI criteria for the surface water samples were as follows; low (HEI < 150), medium (HEI = 150 to 300) and high (HEI > 300). For the groundwater samples, the criteria was: low (HEI < 40), medium (HEI = 40 to 80) and high (HEI > 80). Using this scheme, 55, 36 and 9% of surface water samples showed low, medium and high contamination, respectively with respect to heavy metals, whereas, 50, 40 and 10% of the groundwater samples showed as less, moderately and highly contaminated (Mohammad et al., 2010). MPI is computed to analyze the status of the heavy metal contamination in the environment. MPI is calculated according to Usero et al. (1997) using the given equation:

$$MPI = (C1 \times C2 \times \cdots \times Cn)^{1/n} \quad (6)$$

Where Cn is the concentration of the metal *n* in the sample

Concentrations of metals in water were used to assess human exposure through oral intake and bath. The total HI resulting from exposure to metals through water ranged from 0.64 to 0.66 for adults. In children, HI levels increased between 1.87 and 1.85 up-and downstream river areas, respectively (Renato et al., 2014). The non-cancer risk associated with the single oral exposure to Ti already exceeded the safety level at the upstream area (HQ = 1.38). Arsenic (As) was another element of concern. Although Renato et al. (2014) revealed that As levels were below the safety level, relatively high values of HQ associated with As exposure were also observed. The presence of As, a natural occurring element, may also be attributed to anthropogenic activities, such as the use of herbicides (Christ et al., 2012).

The health risk for heavy metals in seafood is usually quantified by the target hazard quotient (THQ) (Storelli, 2008). The THQ as shown in equation 1 is defined as the concentration of heavy metals divided by a reference dose (RfD). If the THQ is less than 1, the seafood has no health risk. Conversely, the health risk should be considered. Based on the THQ equation and the RfDs of heavy metals published by the United States Environmental Protection Agency (USEPA), the safety limits of Cr, Cu, Zn, Cd, Hg, As and Ni in seafood were 2.9, 39, 292, 1.0, 0.1, 2.9 and 19 mg/kg ww, respectively (USEPA, 2012). Body weight (55.9 kg) and daily consumption amounts of seafood (57.5 g/day) were obtained from the survey conducted by Wang et al. (2005). However, the RfD of Pb is not considered by the USEPA. Thus the consumptive standard of Pb in aquatic organisms (0.5 mg/kg ww) published by the General Administration of Quality Supervision, Inspection and Quarantine of China (AQSIQ) is used in this review (AQSIQ, 2001). Based on the safety limits of heavy metals, consumption levels of Pb and As in most mollusks from Hong Kong exceeded the criteria (Fang et al., 2008). Concentrations of heavy metals in fish from northwestern and southern Hong Kong all met the consumption standards (Cornish et al., 2007). Heavy metal levels in most seafood from Lingdingyang were higher than the safety limit (Shuai-Long Wang, 2013).

A study done by Mishra et al. (2007) in the Trans-Thane Creek area of Mumbai, measured the trace element in different types of marine organisms and reported the HQ values of 0.01 (50th percentile) and 0.005 (95th percentile) in case of the ingestion of Cd. The same study also revealed lower HQ values for Cr, Ni, Zn and Cu and suggested that consumption of fish samples were within the safe limit (Mishra et al., 2007). Similar to the findings, Tu et al. (2008) worked on the concentration of Cr, Cu, Zn and Cd, and measured HQ values of less than 1 which indicated that the local residents were not exposed to potential risk via consumption of shrimp. On the other hand, Schmitt et al. (2006) reported a higher range of HQ values for Cd (0.1 to 0.5) and Zn (0.1 to 12.6) in carp fishes. Samples of black-chin Tilapia, collected from Sukumo lagoon of Ghana, were analyzed for the concentration of heavy metals and the calculated values of HI indicated that the Tilapia did not pose any health risk to humans (Laar et al., 2011).

Heavy metal pollution of soil is regarded as one of the severe environmental challenges in many countries of the world (Facchinelli et al., 2001). Concentrations of As, Cd, Ni and Pb in the soil are among the heavy metals investigated. People experienced higher exposure to As, Cd, Ni and Pb due to their high concentrations in the soil under investigation or low RfD values, whereas they had little exposure to other four heavy metals (Cr, Cu, Zn and Hg). For instance, in the surrounding area of the Chenzhou lead–zinc mine in China, the HQ value of As, Cd, Ni and Pb accounted for 25.8, 13.8, 3.5, and 54.0% of the entire HI value, respectively. By contrast, the total percentage of the other four heavy metals for the entire HI value was 0.2%.

Generally, the total hazard quotients of Pb, Ni, Cd and As accounted for 98.6% of the full HI value in the surrounding area of the Dabaoshan multi-metal mine (Zhiyuan Li et al., 2014). An emphasis was particularly given to Arsenic due to its reported cases of poisoning

and cancer related issues in the region. The carcinogenic risk values for As at some mining areas even exceed 1×10^{-4}. As a whole, these carcinogenic risk levels are unacceptable or close to unacceptable limit. For every mining area, the carcinogenic risks of As for different populations vary greatly, generally in the order of adult females > adult males > children. The reason that the carcinogenic risk for children is less than that for adults lies in the shorter duration of exposure for children. Average As carcinogenic risk values (standard deviation) for antimony, coal, copper, gold, and lead–zinc mining areas are; 5.8×10^{-4} (7.6×10^{-4}), 1.3×10^{-5} (6.9×10^{-6}), 4.7×10^{-5} (7.1×10^{-5}), 1.1×10^{-5} (7.7×10^{-6}), and 1.7×10^{-4} (2.0×10^{-4}), respectively (Zhiyuan Li et al., 2014).

Exposure assessment in air

Not much emphasis was given to assess the risk of exposure of humans to heavy metals by air, as much literature gave emphasis to water and soil by ingestion and dermal (skin). Humans can become exposed to heavy metals in dust through several routes which include ingestion, inhalation, and dermal absorption. In dusty environments, it has been estimated that adults could ingest up to 100 mg dust/day (Hawley, 1985). Children are usually exposed to greater amounts of dust than adults (Centers for Disease Control and Prevention (CDCP), 2005). Exposure to high levels of heavy metals can result in acute and chronic toxicity, such as damage to central and peripheral nervous systems, blood composition, lungs, kidneys, liver, and even death. Lead levels in dust have been significantly associated with Pb levels in children's blood (Lanphear and Roghmann, 1997), and a blood lead level (BLL) greater than an intervention level of 10 µg Pb/dl has been associated with a decrease in IQ (CDCP, 2005). According to Anna et al. (2008), the potential health risk to children at all locations was eight times greater. This was partly attributed to the higher ingestion rate used (200 mg/kg/day) in estimating the risk and the smaller body size. Overall, the accumulative risks due to the metals are a major concern (HI > 1) at all locations except for the locations studied.

GAP IN GENERAL HEALTH RISKS ASSESSMENT

In developed and developing countries of the world, air pollution is increasing at alarming rate prompting the industrialized nations to impose a special tax on industries whose emission is above the approved values by the government. Significant amount of toxic heavy metals had been found in air and dust, especially in industrial areas, and incineration of electronic wastes containing chips, capacitors, and diodes. But much was only given to oral and dermal routes of exposure.

Also, target hazard quotient (THQ) is widely employed to evaluate the health risk, it has several apparent weaknesses among which are: (1) Only suspected targets are considered and determined while the other potential hazardous pollutants are ignored and not analyzed; (2) The relationship or mutual effects of different pollutants are ignored by the THQ, such as, lower pH values which results in precipitation of toxic metals in water. Also, Selenium (Se) can diminish or lessen the toxicity of As and Hg, but few investigations have taken Se into consideration when the health risk of heavy metals is evaluated (Peterson et al., 2009; Ouédraogo and Amyot, 2013), there is a significant correlation between As and Au in soil and water samples obtained from mining areas; (3) The toxicities of heavy metals mainly depend on their bioavailability. For example, As is believed to be one of the most hazardous substances. However, As in fish is mainly present as non-toxic arsenobetaine (Zhang et al., 2012; Zhang and Wang, 2012). Levels of methylmercury (MeHg) in aquatic organisms were generally quite low, but it is highly toxic to wildlife (Liu et al., 2012; Sherman et al., 2013). Therefore further risk assessment techniques for heavy metals should be improved, and other physical parameters be incorporated in the analysis.

CONCLUSION

This review gives an overall view on pollution levels and health risks posed by heavy metals in water, soil and fish and provide reasonable evidence on the utmost need to fully assess the risks of heavy metals and other pollutants to safeguard the health of the community. The knowledge of risks assessment shall be a priority considering continuous increase in heavy metal and general environmental pollution globally in water, air and soil. The continuous and/or periodical acquisition of data on the quality of the water bodies is essential for stakeholders in various countries; also data from soil and food substances needs to be studied. Air risks assessment, especially in industrial and populated regions needs to be carried out periodically. This will enhance proper monitoring and ensure safety of the citizens especially children who are more vulnerable to toxicity of heavy metals.

Conflict of Interests

The authors have not declared any conflict of interests.

REFERENCES

Anna O, Leung W, Nurdan S, Duzgoren-Aydin S, Cheung KC, Ming HW (2008). Heavy Metals Concentrations of Surface Dust from e-Waste Recycling and Its Human Health Implications in Southeast China. Environ. Sci. Technol. 42:2674-2680.

AQSIQ (2001). General Administration of Quality Supervision, Inspection and Quarantineof the People's Republic of China. Safety Qualification for Agricultural Product-Safety Requirements for Non-environmental Pollution Aquatic Products (GB18406.4-2001).

Ashraf M, Hussian SS (1982). Chromite occurrence in Indus suture ophiolite of Jijal, Kohistan, Pakistan, in: K.A. Sinha (Ed.), Contemporary Geoscientific Researches in Himalaya Dehra Dun India pp. 129-131.

Barbee JYJ, Prince TS (1999). Acute respiratory distress syndrome in a welder exposed to metal fumes. South Med. J. 92:510-520.

Centers for Disease Control and Prevention (2005), Preventing Lead Poisoning in Young Children. Centers for Disease Control, Atlanta, GA.

Christ O, Charalambous M, Aletrari C, Nicolaidou Kanari M, Petronda P, Ward NI (2012). Arsenic concentrations in ground waters of Cyprus. J. Hydrol. 468(469):94-100.

Cornish AS, Ng WC, Ho VCM, Wong HL, Lam JCW, Lam PKS, Leung KMY (2007). Trace metals and organochlorines in the bamboo shark *Chiloseyllium plagiosum* from the southern waters of Hong Kong, China. Sci. Total Environ. 376:335-345.

Dieter HH, Bayer TA, Multhaup G (2005). Environmental copper and manganese in the pathophysiology of neurologic diseases (Alzheimer's disease and Manganism), Actahydroch. hydrob. 33:72-78.

Edet AE, Offiong OE (2002). Evaluation of water quality pollution indices for heavy metal contamination monitoring, A study case from Akpabuyo- Odukpani Area Lower Cross River Basin (Southeastern Nigeria). Geo. J. 57:295-304.

Enaam JA (2013). Evaluation of Surface Water Quality Indices for Heavy Metals of Diyala River Iraq. J. Nat. Sci. Res. 3(8):63-64.

Fang JKH, Wu RSS, Chan AKY, Shin PKS (2008). Metal Concentrations in Green-lipped mussels (*Pernaviridis*) and rabbitfish (*Siganusoramin*) from Victoria Harbour, Hong Kong after pollution abatement. Mar. Pollut. Bull. 56:1486-1491.

Facchinelli A, Sacchi E, Mallen L (2001). Multivariate statistical and GIS-based approach to identify heavy metal sources in soils. Environ. Pollut. 114:313-324.

Fenglian Fu, Qi W (2011). Removal of Heavy Metal ions from Waste Waters: A review. J. Environ. Manage. 92(3):407-418.

Hawley JK (1985). Assessment of health risk from exposure to contaminated soil. Risk Anal. 5:289-302.

Hinrichsen D, Tacio H (2002). The coming fresh water crisis is already here. Finding the source: The linkages between population and water. Woodrow Wilson International Center for Scholars, Washington, DC, ESCP Publication spring.

Hu X, Zhang Y, Ding ZH, Wang TJ, Lian HZ, Sun YY (2012). Bio accessibility and health risk of arsenic and heavy metals (Cd, Co, Cr, Cu, Ni, Pb, Zn and Mn) in TSP and PM2. 5 in Nanjing, China. Atmos. Environ. 57:146-152.

IARC (1993).Cadmium and cadmium compounds, Beryllium, Cadmium, Mercury and Exposure in the Glass Manufacturing Industry. IARC Monogr. Eval. Carcinogen. Risks-Hum. 58:2119-2378.

Jarup L (2003). Hazards of heavy metal contamination Brit. Med. Bull. 68:167-182.

Jarup L, Hellstrom L, Alfven T, Carlsson MD, Grubb A, Persson B, Pettersson C, Spang G, Schutz A, Elinder CG (2000). Low level exposure-cadmium and early kidney damage: The OSCAR study Occup. Environ. Med. 57:668-672.

Knight C, Kaiser GC, Lailor H, Robothum J, Witter V (1997). Heavy metals in surface water and stream sediments in Jamaica. Environ. Geochem. Health 19:63-66.

Laar C, Fianko JR, Akiti TT, Osae S, Brimah AK (2011).Determination of heavy metals in the black-chin tilapia from the Sakumo Lagoon, Ghana Res. J. Environ. Earth Sci. 3:8-13.

Lanphear BP, Roghmann KJ (1997). Pathways of lead exposure in urban children. Environ. Res. 74:67-73.

Li S, Liu W, Gu S, Cheng X, Xu Z, Zhang Q (2009). Spatio-temporal dynamics of nutrients in the upper Han River basin, China. J. Hazard. Mater. 162(2):1340.

Liang F, Yang SG, Sun C (2011).Primary Health Risk analysis of metals in surface water of Taihu Lake China. B. Environ. Contam. Toxicol. 87(4):404.

Liu CW, Liang CP, Lin KH, Jang CS, Wang SW, Huang YK, Hsueh YM (2007). Bioaccumulation of arsenic compounds in aqua cultural clams (*Meretrixlusoria*) and assessment of potential carcinogenic risks to human health by ingestion. Chemosphere 69:128-134.

Liu JL, Feng XB, Qiu GL, Anderson CWN, Yao H (2012). Prediction of methylmercury uptake by rice plants (*Oryza sativa* L.) using the diffusive gradient in thin films technique. Environ. Sci. Technol. 46:11013-11020.

Lushenko MA (2010). A risk assessment for ingestion of toxic chemicals in fish from Imperial beach, California: San Diego State University.

Miller DJ, Loucks RR, Ashraf M (1991). Platinum-group metals mineralization in the Jijal layered ultramafic–mafic complex, Pakistani Himalayas. Econ. Geol. 86:1093-1102.

Mishra S, Bhalke S, Saradhi IV, Suseela B, Tripathi RM, Pandit GG, Puranik VD (2007). Trace metals and organometals in selected marine species and preliminary risk assessment to human beings in Thane Creek Area, Mumbai. Chemosphere 69:972-978.

Mohammad AH, Bhuiyan MA, Samuel BD, Parvez L, Shigeyuki S (2010). Evaluation of hazardous metal pollution in irrigation and drinking water systems in the vicinity of a coal mine area of northwestern Bangladesh. J. Hazard. Mater. 179:1065-1077.

Nordberg G, Jin T, Bernard A, Fierens S, Buchet JP, Ye T, Kong Q, Wang H (2002). Low bone density and renal dysfunction following environmental cadmium exposure in China. Ambio 3:478-481.

OEHHA (2011). Adoption of the revised air toxics hot spots program technical support document for cancer potency factors.

Ouedraogo O, Amyot M (2013). Mercury, arsenic and selenium concentrations inwater and fish from sub-Saharan semi-arid freshwater reservoirs (Burkina Faso). Sci. Total Environ. 444:243-254.

Ouyang Y, Higman J, Thompson J, Toole OT, Campbell D (2002). Characterization and spatial distribution of heavy metals in sediment from Cedar and Ortega Rivers sub-basin. J. Contam. Hydrol. 54:19-35.

Peterson SA, Ralston NVC, Peck DV, Van Sickle J, Robertson JD, Spate VL, Morris JS (2009). How might selenium moderate the toxic effects of mercury in stream fish of the western US? Environ. Sci. Technol. 43:3919-3925.

Renato IS, Carolina FS, Martí N, Marta S, José LD, Segura-Muñoz S (2014). Metal concentrations in surface water and sediments from Pardo River, Brazil: Human health risks. Environ. Res. 133:149-155.

Robert G, Mari G (2003). Human Health Effects of Metals, US Environmental Protection Agency Risk Assessment Forum, Washington, DC.

Said M, Tahir SM, Sardar K (2011). Health risk assessment of heavy metals and their source apportionment in drinking water of Kohistan region, northern Pakistan. Microchem. J. 98:334-343.

Schmitt C, Brumbaugh W, Linder G, Hinck JE (2006). A screening-level assessment of lead, cadmium, and zinc in fish and crayfish from northeastern Oklahoma, USA. Environ. Geochem. Health 28:445-471.

Sherman LS, Blum JD, Franzblau A, Basu N (2013). New insight into biomarkers of human mercury exposure using naturally occurring mercury stable isotopes. Environ Sci. Technol. 47:3403-3409.

Shuai-Long W, Xiang-Rong X, Yu-Xin S, Jin-Ling L, Hua-Bin L (2013). Heavy metal pollution in coastal areas of South China: A review. Mar. Pollut. Bull. 76:7-15.

Storelli MM (2008). Potential human health risks from metals (Hg, Cd, and Pb) and polychlorinated biphenyls (PCBs) via seafood consumption: Estimation of target hazard quotients (THQs) and toxic equivalents (TEQs). Food Chem. Toxicol. 46:2782-2788.

Strachan S (2010). Heavy metal. Curr. Anaesth. Crit. Care 2:44-48.

Tu NVC, Ha NN, Ikemoto T, Tuyen BC, Tanabe S, Takeuchi I (2008). Regional variations in trace element concentrations in tissues of black tiger shrimp *Penaeus monodon (Decapoda: Penaeidae*) from South Vietnam. Mar. Pollut. Bull. 57:858-866.

USEPA (1989). United States Environmental Protection Agency. Risk Assessment Guidance for Superfund (Volume 1) - Human Health

Evaluation Manual Part A Interim Final.EPA/540/1-89/002.Office of Emergency and Remedial Response, Washington, DC, USA.
USEPA (1996) Quantitative Uncertainty Analysis of Superfund Residential Risk Pathway Models for Soil and Ground water: White Paper. Office of Health and Environmental Assessment, Oak Ridge TN USA.
USEPA (2011). USEPA regional screening level (RSL) summary table. Washington, DC.
USEPA (2012). Waste and cleanup risk assessment. http://www2.epa.gov/risk/waste-and-cleanup-risk-assessment
Usero J, González-Regalado E, Gracia I (1997). Trace metals in the bivalve mollusks *Ruditapes decussatus* and *Ruditapes philippinarum* from the Atlantic coast of southern Spain. Environ. Int. 23:291-298.
Wang XL, Sato T, Xing BS, Tao S (2005). Health risks of heavy metals to the general public in Tianjin, China via consumption of vegetables and fish. Sci. Total Environ. 350:28-37.
Wasserman G, Liu X, Parvez F, Ahsan H, Levy D, Litvak PF, Kline J, Geen AV, Slavkovich V, Lolacono N, Cheng Z, Zheng Y, Graziano J (2006). Water manganese exposure and children's intellectual functions in Araihazar, Bangladesh Environ. Health Perspect. 114:124-129.
Wu B, Zhao DY, Jia HY, Zhang Y, Zhang XX, Cheng SP (2009). Preliminary Risk Assessment of trace metal pollution in surface water from Yagtze River in Nanjing Section, China. B. Environ. Contam. Toxicol. 82(4):405.
Zhang W, Wang WX (2012). Large-scale spatial and interspecies differences intrace elements and stable isotopes in marine wild fish from Chinese waters. J. Hazard. Mater. 215:65-74.
Zhang, W, Huang, L, Wang, WX (2012) Biotransformation and detoxification of inorganic arsenic in a marine juvenile fish *Terapon jarbua* after waterborne and dietborne exposure. J. Hazard. Mater. 221:162-169.
Zhiyuan Li, Zongwei M, Tsering JV, Zengwei Y, Lei H (2014). A review of soil heavy metal pollution from mines in China: Pollution and Health risk assessment. Sci. Total Environ. 468(469):843-853.

academicJournals

Vol. 9(11), pp. 211-222, November, 2015
DOI: 10.5897/AJPAC2015.0656
Article Number: EE1CD6956202
ISSN 1996 - 0840

http://www.academicjournals.org/AJPAC

African Journal of Pure and Applied Chemistry

Full Length Research Paper

Synthesis, characterization and photocatalytic activity of $MnO_2/Al_2O_3/Fe_2O_3$ nanocomposite for degradation of malachite green

Haile Hasana Logita[1]*, Abi Tadesse[2] and Tesfahun Kebede[2]

[1]Chemistry Department of Hawasa College of teacher education, Ethiopia.
[2]Chemistry Department of Haramaya University, Ethiopia.

Received 1 October, 2015; Accepted 22 October, 2015

New nanocomposite $MnO_2/Al_2O_3/Fe_2O_3$ photocatalyst was successfully synthesized by sol-gel method using metal salts as precursors in the presence of acid catalyst. The as-synthesized samples were characterized by X-ray diffraction (XRD), Fourier transform infrared (FTIR), atomic absorption spectroscopy (AAS) and UV-Vis diffuse reflectance spectroscopy. Elemental analyses of the as-synthesized samples were similar to those expected from the initial concentrations of the solutions used during synthesis. The x-ray diffraction pattern indicated that all as-synthesized samples had a crystal size with a rhombohedral structure and finest particle size of the catalyst (20.096 nm) was obtained at 400°C calcination temperature. The band gap energy of the $MnO_2/Al_2O_3/Fe_2O_3$ photocatalyst was calculated to be 1.97 eV and indicated that the as-synthesize sample had high photoabsorption property in the visible light region. Fourier transform infrared spectra confirmed the presence of hydroxyl group and Fe-O bond vibration in the catalyst. Experimental result of the $MnO_2/Al_2O_3/Fe_2O_3$ photocatalyst calcined at 400°C in 180 min (the molar ratio of 10 wt% Mn/15 wt% Al/75 wt% Fe) exhibited high photocatalytic activity of 92.89% under visible light irradiation. This may be due to the coupling effect of semiconductors, small particle size of catalyst and low electron-hole pair recombination on the surface of the catalyst. The pseudo-first-order rate constants of MG dye degradation in the presence of the catalyst were calculated as 4×10^{-4}, 6.56×10^{-3} and 1.0×10^{-2} min^{-1} under no light irradiation, UV and visible light irradiation, respectively.

Key words: Malachite green, nanoparticles, photocatalysis, sol-gel synthesis, ternaryoxides.

INTRODUCTION

Heterogeneous photocatalysis has become an alternative treatment method for degradation of organic pollutants from wastewater, which has the ability to mineralize organic compounds. In fact, photocatalysis can greatly contribute to the remediation of those environmental pollutants into environmental friendly species: CO_2, H_2O

*Corresponding author. E-mail: julianacr@epamig.ufla.br.

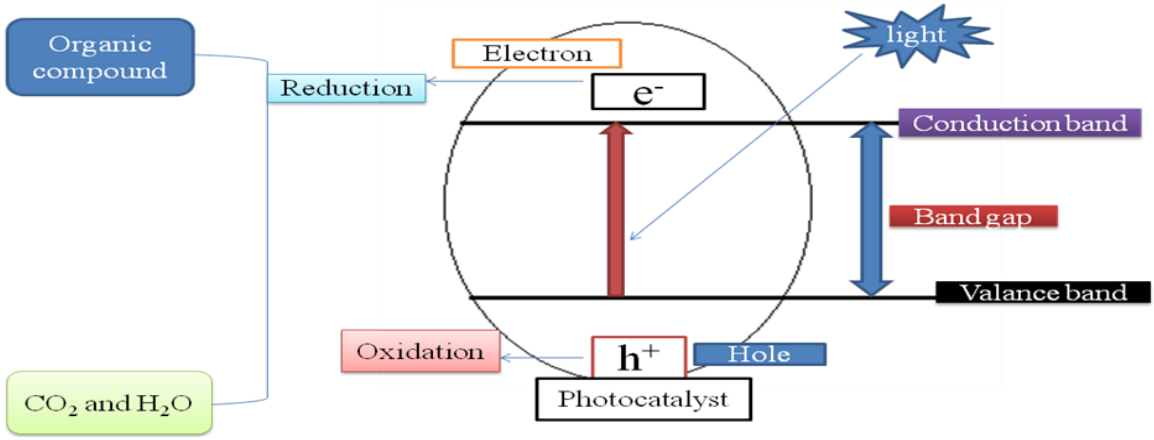

Figure 1. Schematic diagram of photocatalytic process initiated by photon acting on the semiconductor.

or other oxides, halide ion, phosphate (Sakthivel et al., 2005; Brijesh et al., 2008; Gomathi et al., 2009). The semiconducting metal oxides like iron oxide (Fe_2O_3) nanomaterials exhibit promising photocatalytic activities due to their environmental friendly behavior, low catalyst cost, high specific surface area, high crystallinity and solar energy application (Leland and Bard, 1987; Zhao et al., 2009; Bharathi et al., 2010) and thus, could be an alternative material for environmental application and wastewater treatment (Rhoton et al., 2002; Lei et al., 2006, 2007; Wang et al., 2009). However, the photocatalytic activity of the iron oxide is depending on the particle size, which is difficult to synthesize nano-sized iron oxide by conventional method and to control its crystal size in the photocatalyst (Park et al., 2010). This is due to the agglomeration of nano-particles in the aqueous solution, which causes the reduction of photocatalytic efficiency. This therefore warrants some smart strategy for use of iron oxide catalyst. One certain way to overcome this drawback is to apply innovative synthetic method of iron oxide nanoparticles of the catalysts that can be easily dispersed in organic medium and homogenously loaded on to the supported materials.

Many studies have continuously tried to improve the photocatalytic activity of iron oxide by coupling of different semiconductor oxide nanoparticles (Baldrian et al., 2006; Laat and Le, 2006; Kitis and Kaplan, 2007; Zelmanov and Semiat, 2008). Thus Al_2O_3/Fe_2O_3 supported photocatalyst has shown a better photocatalytic activity (El-Moselhy, 2009; Li et al., 2010; Pattanayak, 2010; Jia-feng et al., 2011). These new composite allows for the decreasing of the particle size of the catalyst (Karakassides and Gournis, 2003). It is an important material for the application of heterogeneous photocatalysis (Cordier et al., 2006). However, the photocatalytic activity of Al_2O_3/Fe_2O_3 nanocomposite is still not satisfactory for degradation of organic pollutants in wastewater because of its low electron-hole separation. This may be due to similar ionic radii and same charge of the materials. Subsequently complete substitutions occur between aluminum (III) oxide and iron (III) oxide nanoparticles and no structural defect could be expected (Neiva et al., 2009). Currently, nano-manganese (IV) oxide (MnO_2) has received a great potential application in environmental protection and degradation of organic pollutants in wastewater (Mitta et al., 2009; Su, 2010). It is a promising material for heterogeneous photocatalyst as a new generation environmental friendly catalyst. This is due to its high specific surface area, crystallinity, ability to disintegrate water molecule into hydrogen and hydroxide ions (Kang et al., 2007; Chu and Zhang, 2009). Based on these advantages MnO_2 semiconductor was chosen as an assistant component of photocatalyst to improve the photocatalytic activities of binary Al_2O_3/Fe_2O_3 nanocomposite. Therefore, in this study the triple oxide photocatalyst of $MnO_2/Al_2O_3/Fe_2O_3$ was used in photodegradation of MG dye in aqueous solution by using atomic absorption spectroscopy (AAS), X-ray diffraction (XRD), Fourier transform infrared (FTIR) and UV/Vis spectrometric techniques. A schematic representation of the photocatalytic process is represented in Figure 1.

MATERIALS AND METHODS

Synthesis of photocatalyst

The $MnO_2/Al_2O_3/Fe_2O_3$ ternary mixed nanoxide powder was prepared by sol-gel method. The sol corresponded to total volume ratio of metal, butanol, deionized water and nitric acid ratio of 1:20:4:0.1. In each case, ferric nitrate nanohydrate and aluminum nitrate nanohydrate were dissolved in stoichiometric amounts of water, 69% HNO_3 and butanol then mixed with vigorous stirring. $KMnO_4$ and $Na_2S_2O_3.5H_2O$ were mixed with each other and dissolved in double dionized water to form dark-brown MnO_2 solution. Subsequently, the dark brown MnO_2 solution was added drop wise into the mixture of aluminum oxide/iron oxide solution through stirring for 30 min at room temperature. The prepared sol was left to stand for the formation of gel. After the gelation was completed, the gel was aged for 5 days at room temperature and

Table 1. Designation of the as-synthesized powders.

Sample code	Precursor composition in g	%Composition at different calcination temperature
T_1	Al-3.64/Fe-36.46	90% Fe/10 % Al/0% Mn calcined at 400°C
T_2	Mn-0.83/Al-5.46/Fe-32.41	80% Fe/15 %Al/5% Mn calcined at 400°C
T_3	Mn-1.66/Al-5.64/Fe-30.38	75% Fe/15 % Al/10%Mn calcined at 400°C
T_4	Al-3.64/Fe-36.46	90% Fe/10 % Al/0% Mn calcined at 600°C
T_5	Mn-0.83/Al-5.46/Fe-32.41	80% Fe/15 %Al/5% Mn calcined at 600°C
T_6	Mn-1.66/Al-5.64/Fe-30.38	75% Fe/15 % Al/10% Mn calcined at 600°C

sample was dried at 75°C for 36 h. After grinding the dried samples, they were calcined at 400 and 600°C for 3 h at the different molar ratios. The different molar ratios of MnO_2:Al_2O_3:F_2O_3 are summarized in Table 1.

Characterization

Elemental composition

The elemental compositions of the as-synthesized powder were analyzed by flame atomic absorption spectrophotometer. 0.01 g of the as-synthesized powders were digested with conc. HNO_3 (7 ml), conc. HCl (4 ml) and H_2O_2 (2 ml) using acid digestion tube till clear solution appeard. The samples of Fe (III) and Mn (IV) solutions were transferred to 100 and 50 ml volumetric flasks and brought to volume using de-ionized water; triplicate solutions of iron and manganese were read from 100 and 50 ml volumetric flasks, respectively. Stock standard solutions of 1000 mg/L Fe and Mn were prepared by dissolving 0.14 and 0.36 g of corresponding salts in de-ionized water, respectively and series standard solutions were prepared to plot the calibration curves of the metals by appropriate dilution.

X-ray diffraction study

In order to determine the crystal phase composition of as-synthesized photocatalysts, all powder catalysts were ground to fine particles and analyzed by a BRUKER D8 Advance XRD, AXS GMBH, Karlsruhe, West Germany X-ray diffractometer (XRD) equipped with a Cu target for generating a Cu Kα radiation (λ = 0.15406 nm) at GSE. The accelerating voltage and the applied current were 40 kV, 30 mA, respectively. The instrument was operated under step scan mode with step time and degree (2θ) of 1 s and 0.020°, respectively for the range of 4 to 64°.

UV-Visible diffuse absorbance

For the estimation of absorption edge of the as-synthesized photocatalyst, UV-Visible diffuse absorption was measured using SP65 spectrophotometer at Addis Ababa University research laboratory. As-synthesized sample was dissolved in hot methanol then the UV-Visible diffuse absorbance of the powder was recorded at 200 to 800 nm range to determine the band gap of the photocatalyst.

Fourier transform infrared study

As-synthesized nanopowder was characterized using FTIR (SHIMIDAZU) instrument. Ten mg (dry mass) of the photocatalyst was thoroughly mixed with 100 mg (dry mass) of KBr and ground to a fine powder. A transparent disc was formed by applying a pressure in moisture-free atmosphere. The IR absorption spectrum was recorded between 400 and 4000 cm^{-1}.

Photocatalytic degradation studies

Photocatalytic activities of the as-synthesized powder were evaluated by decolorization of malachite green dye in aqueous solution. The experiments were carried out in the presence of UV and Visible light irradiation without any catalyst (blank), with catalyst in dark and in the presence of $MnO_2/Al_2O_3/Fe_2O_3$ photocatalyst. The photocatalytic reactor consists of a Pyrex glass beaker with an inlet tube for provision of air purging during photocatalysis and outlet tube for the collection of samples from the beaker as shown in Figure 2. Reaction was set up by adding 0.15 g of the as-synthesized powder into 100 ml of MG solution (25 mg/L) in the Pyrex glass beaker of 250 ml volume and the suspension was magnetically stirred in dark for 30 min to obtain adsorption/desorption equilibrium before irradiating the light in the beaker. Before illumination of the samples by UV or visible radiations, air/oxygen was purged into the solution with the help of a porous tube at hand purging in order to keep the suspension of the reaction homogenous. During the reaction, the solution was maintained at room temperature and the distance of the lamp from the solution was 9 cm and its intensity was recorded to be 8.25 MW/cm^2. Then, the light source was activated; 10 ml of the sample was withdrawn at 20 min time interval over irradiation time for 180 min. The suspension was centrifuged at 3000 rpm for 10 min and filtered to remove the catalyst particles before measuring absorbance. The absorbance of the clear solution was measured at a λ_{max} of 620 nm for quantitative analysis. The UV lamp with a definite power 12 W, 230 V and 50 Hz frequency was employed as UV light source, and incandescent bulb was used as visible light source with a definite power of 40 W, 220 V and 60 Hz frequency. Percentage degradation of MG dye was calculated using the following relation:

$$\%\,\text{Degradation} = \frac{A_o - A_t}{A_o} \text{x} 100$$

Where: A_0 is absorbance of dye at initial stage, A_t is absorbance of dye at time t.

RESULTS AND DISCUSSION

Characterization

Elemental composition

Elemental compositions of the as-synthesized samples

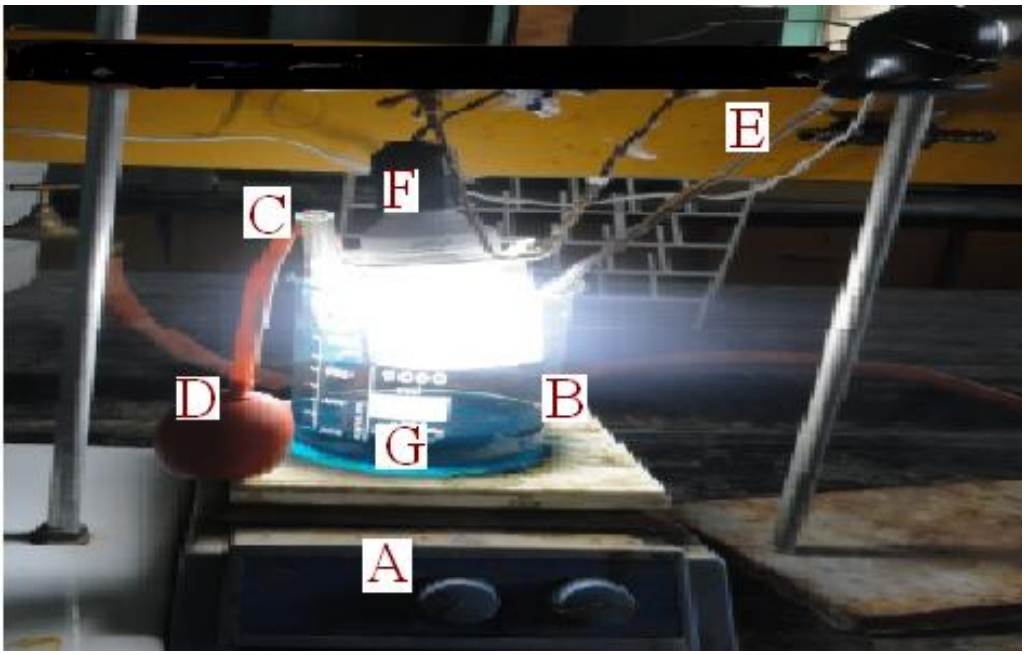

Figure 2. Schematic diagram of photocatalytic reaction in pyrex glass beaker under visible light irradiation. A. Hot plate (B) Pyrex glass beaker containing the solution (C) Inlet tube for air purging (D) Porous tube (E) Outlet tube for collecting sample solutions at 20 min time interval (F) Radiation source (G) Magnetic stirrer.

Table 2. Percentage composition of Iron oxide and Manganese oxide were calculated from as-synthesized powders

Sample name	%Fe[a]	%Fe[b]	%Mn[a]	%Mn[b]	%Al[a]	%Al[b]
Al_2O_3/Fe_2O_3	90	90.50	0.00	0.00	10	-
$MnO_2/Al_2O_3/Fe_2O_3$	80	81.58	5.00	4.66	15	-
$MnO_2/Al_2O_3/Fe_2O_3$	75	75.79	10	10.62	15	-

[a]initial percentage composition of as-synthesized sample, [b]percentage composition of as-synthesized sample calculated from the AAS and %Al[b] not determined.

were analyzed through flame atomic absorption spectrophotometer. Triplicate sample solutions were carried out together with blank solution on each sample as shown in Table 2. The standard solutions of iron and manganese metals were analyzed and the calibration curves were plotted on standard solution versus absorbance. Accordingly, the percentage composition of iron and manganese oxide analyzed by AAS was similarly to those expected from the initial concentration of the solution that was measured during the synthesis.

X-ray diffraction analysis

The crystallinity of the Al_2O_3/Fe_2O_3 and $MnO_2/Al_2O_3/Fe_2O_3$ photocatalysts synthesized by the sol-gel method at different molar ratios were studied by XRD after calcination at 400 and 600°C. The broad diffraction peaks presented in Figures 3 and 4 clearly revealed that all as-synthesized samples were nanosized crystals with a rhombohedral structure of hematite. Similarly, weak diffraction peaks presented in all as-synthesized samples at 2θ values of 24.1, 35.6, 40.8, 49.3, 54.0 and 62.3 were due to Fe_2O_3, and these correlated with the reported data of hematite (Park et al., 2010). However, the XRD data did not show any presence of Al_2O_3 and MnO_2 particles in the ternary mixed oxide system which confirmed that Al (III) and Mn (IV) enter into the Fe_2O_3 lattice substitution. In fact, ionic radius of Mn (IV) of 53 pm and Al (III) of 54 pm is similar to that of ionic radius (55 pm) of Fe (III) thus the substitution in the matrix of Fe_2O_3 is a favorable process. As a result, Al (III) ions and Mn (IV) ions can substitute Fe (III) lattice site to form a stable solid solution. The average crystallite sizes of the as-synthesized powders were calculated using Debye Scherer equation (Yan et al., 2010):

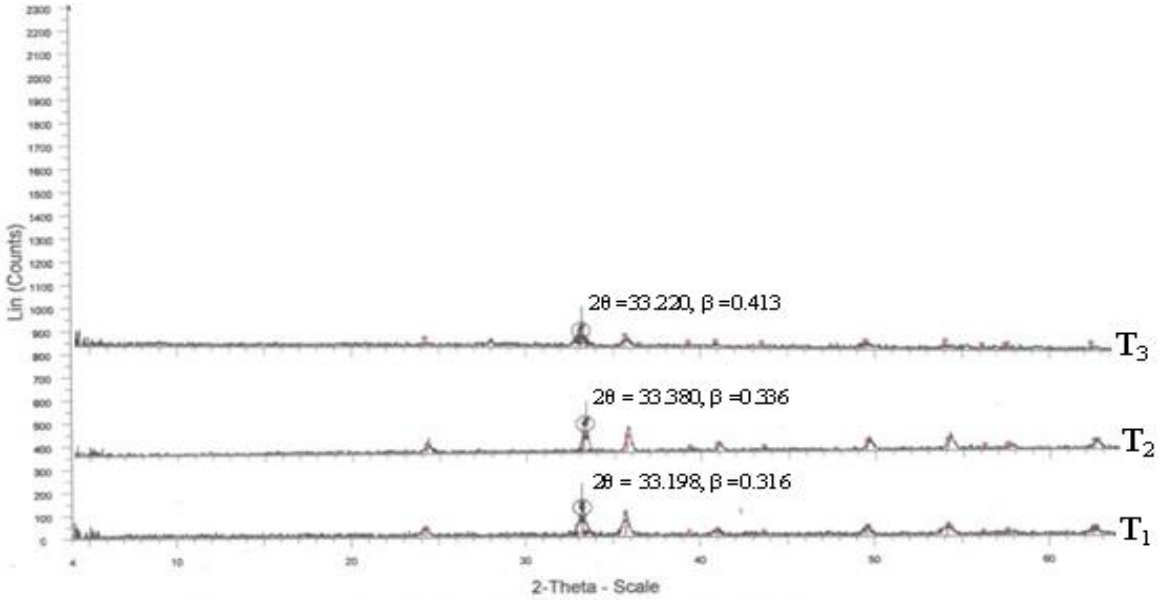

Figure 3. X-ray powder diffraction of the photocatalyst after calcination at 400°C

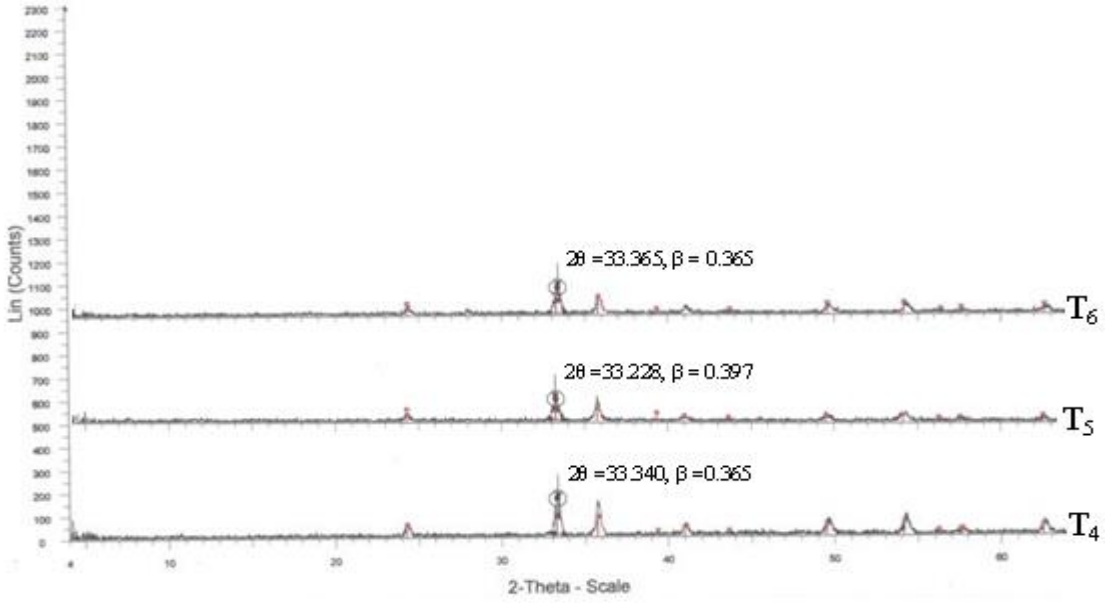

Figure 4. X-ray powder diffraction of the photocatalyst after calcination at 600°C.

$$D = \frac{K\lambda}{\beta cos\theta}$$

Where D is the crystal size (nm), λ is X-ray wavelength corresponding to the Cu target Kα irradiation (0.15406 nm), and β is full width at half maximum (FWHM) of the peak in radian, K = 0.90 is a constant coefficient of spherical shape and θ is the (Bragg angle) corresponding to the diffraction angle. The calculated average crystallite sizes (D) of the photocatalysts are given in Tables 3 and 4.

As shown from the tables, all the as-synthesized powders were nanosized crystal and sample T_3 of Mn-1.66/Al-5.64/Fe-30.38 calcined at 400°C has the smallest crystalline size and hence a high surface area. This sample was selected for UV-Visible and FTIR characterization and photodegradation experiment of malachite green.

Table 3. Average particle size (D) of the as-synthesized nanopowder calcined at 400°C.

Sample code	Precursor composition (g)	2θ(Degree)	β(Radian)	D(nm)
T_1	Al-3.64/Fe-36.46	33.198	0.316	26.310
T_2	Mn-0.83/Al-5.46/Fe-32.41	33.380	0.336	24.760
T_3	Mn-1.66/Al-5.64/Fe-30.38	33.220	0.413	20.096

Table 4. Average particle size (D) of the as-synthesized nanopowder calcined at 600 ^{0}C

Sample code	Precursor composition (g)	2θ(Degree)	β(Radian)	D(nm)
T_4	Al-3.64/Fe-36.46	33.340	0.365	24.531
T_5	Mn-0.83/Al-5.46/Fe-32.41	33.228	0.397	24.530
T_6	Mn-1.66/Al-5.64/Fe-30.38	33.365	0.365	22. 620

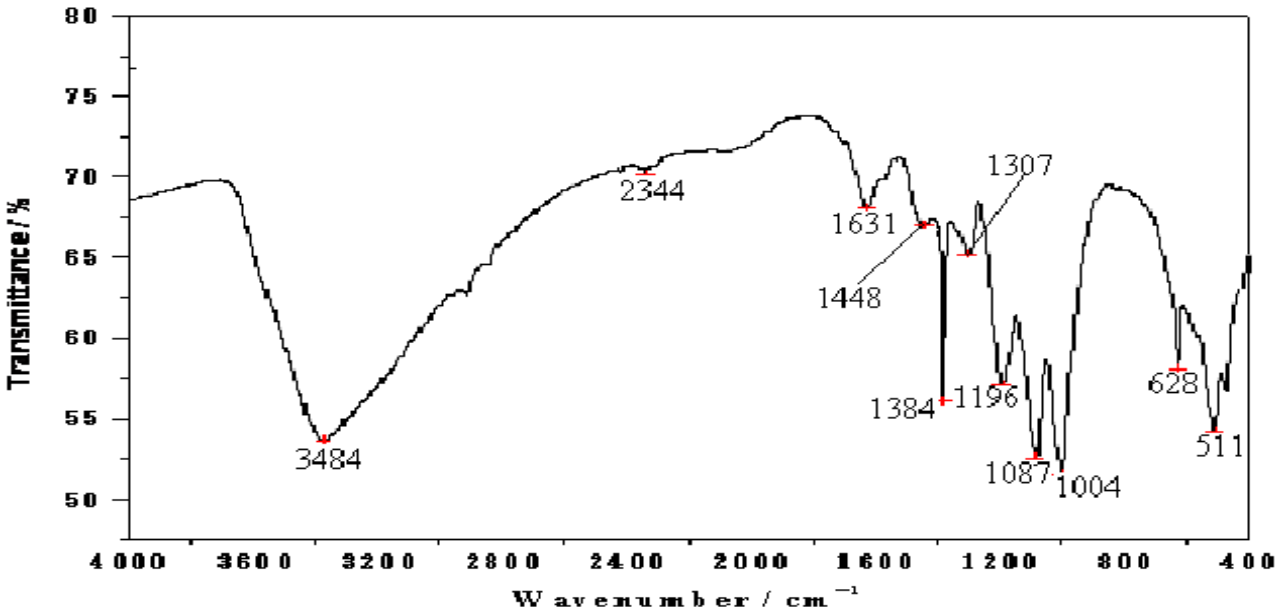

Figure 5. FTIR spectra of $MnO_2/Al_2O_3/Fe_2O_3$ nanopowder before calcinations.

FTIR analysis of photocatalysts

The FTIR spectra of the nanocomposite $MnO_2/Al_2O_3/Fe_2O_3$ photocatalyst prepared by sol-gel method before and after calcination are presented in Figures 5 and 6. The intense band at 3384 cm^{-1} may be due to the stretching modes of -OH group from adsorbed water in the sample. The band observed at 1631 cm^{-1} can be assigned to the bending vibration of free water molecule; while bands observed at 2344, 1448, 1384 and 1307 cm^{-1} may be attributed to -CH, $-CH_2$ and $-CH_3$ functional groups. Sharp peaks at 1196, 1087 and 1004 cm^{-1} may be due to C-O stretching vibration of primary alcohol, which was used to support the sol gel synthesis. The absorption peak observed at 628 cm^{-1} could be associated with the presence of Fe-O bond in the catalyst structure. The band at 511 cm^{-1} may indicate the presence of iron oxide in $MnO_2/Al_2O_3/Fe_2O_3$. Broad band at 3440 cm^{-1} may be due to the stretching vibration of -OH from adsorbed water in the crystal sample. The band observed at 1623 cm^{-1} could be assigned to the bending vibration mode of free water molecule. Weak bands observed at 2925, 2850 and 1384 cm^{-1} may be due to C-H stretching vibrations of primary alcohol. The peaks at 486 and 553 cm^{-1} may be attributable to the Fe-O vibration bond of hematite in the $MnO_2/Al_2O_3/Fe_2O_3$ nanocomposite of rhombohedral structure (Li et al., 2007).

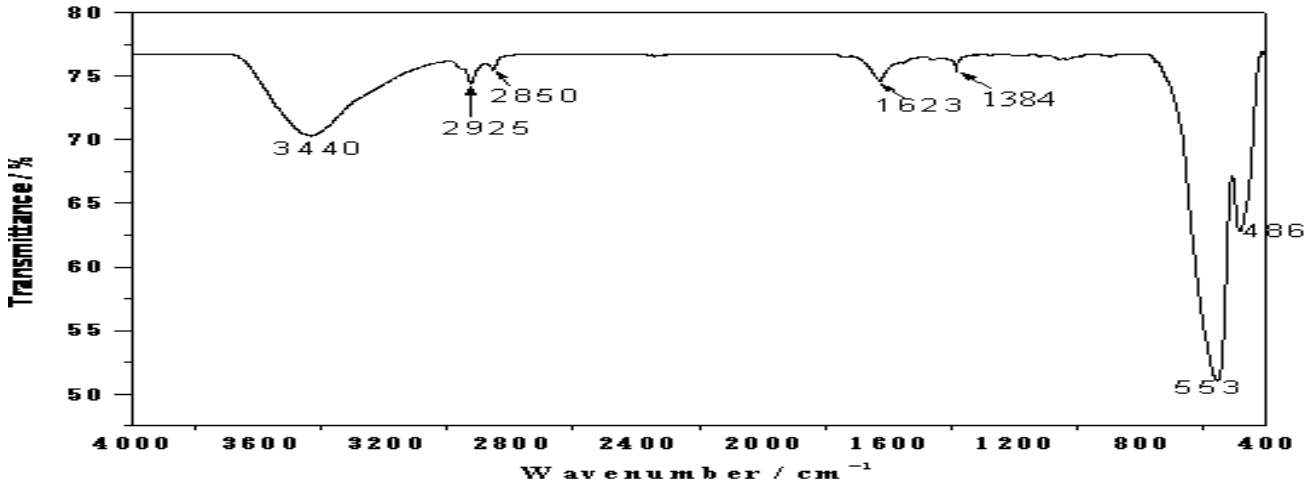

Figure 6. FTIR spectra of $MnO_2/Al_2O_3/Fe_2O_3$ nanopowder after calcination at 400°C.

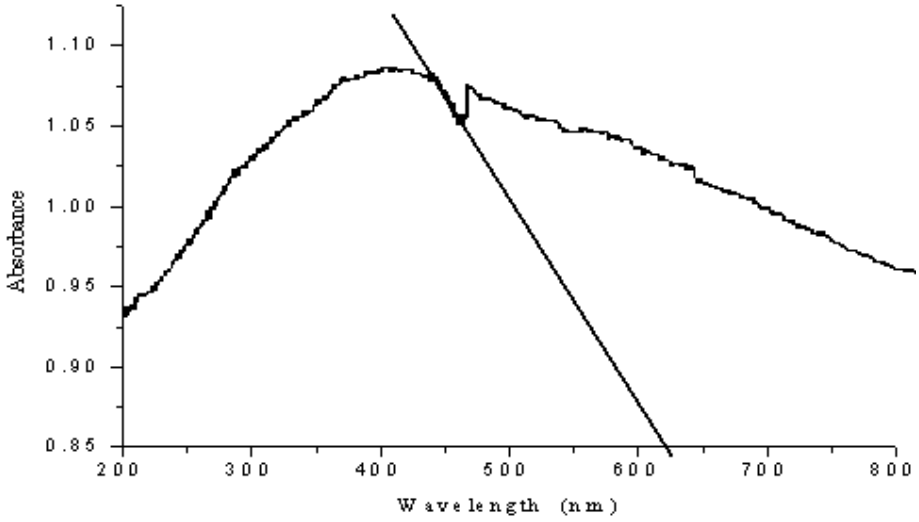

Figure 7. UV-Visible absorption spectra of as-synthesized photocatalyst $MnO_2/Al_2O_3/Fe_2O_3$.

Generally, from the FTIR spectra shown in the Figure 6, it can be concluded that intensities of most of the vibration peaks have eventually decreased during the conversion process of the precursors into the $MnO_2/Al_2O_3/Fe_2O_3$ photocatalyst. This change may be attributed to the decomposition of organic substances present before the calicination and the formation of crystalline phase during the process of heat treatment. As a consequence, only the vibration band corresponding to a Metal-Oxygen bond could be detected below 700 cm^{-1} (Torres-Martinez et al., 2010).

UV-Visible diffuse absorption edge

The optical absorption property of the material and migration of the light induced electrons and holes are considered as the key factor controlling the photocatalytic reaction. Of course, these migrations are relevant to the change in the electronic structure and characteristic of the material. The UV-Vis diffuse reflectance spectra of the as-synthesized $MnO_2/Al_2O_3/Fe_2O_3$ nanopowder obtained by the sol gel method and calcined at 400°C for 3 h was subjected to strong photoabsorption in the visible light region as shown in Figure 7. On the basis of this, the band gap energy (E_g) of the material can be calculated using the following formula (Chien-Tsung, 2007):

$$E_g(eV) = \frac{1240}{\lambda}$$

Where E_g is band gap energy in electron volt, λ is

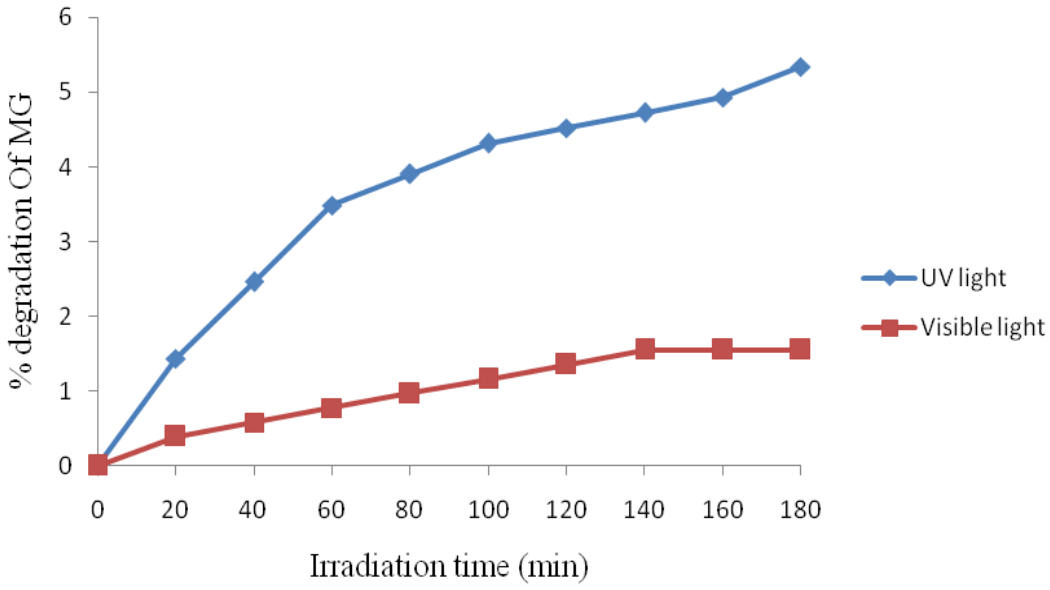

Figure 8. Plots of percentage degradation of MG dye as function of time under UV and Visible light irradiations in blank solution (without catalyst).

wavelength (nm) corresponding to absorption edge.

Accordingly, the band gap absorption edge of the $MnO_2/Al_2O_3/Fe_2O_3$ photocatalyst was the determined to be 630 nm, and thus corresponds to reduced band gap energy of 1.97 eV compared with E_g(eV) of Fe_2O_3 (2.3 eV). Such a reduction in the band gap energy may be the result of positive change in the crystallite phase and the size of ternary mixed oxide and defect of the composite structure. Therefore, the result indicates that the $MnO_2/Al_2O_3/Fe_2O_3$ nanopowder can have a suitable band gap for photocatalytic degradation of organic pollutant under visible light irradiation.

Photocatalytic degradation study

The photocatalytic activity of as-synthesized nanomaterial was evaluated by the degradation of malachite green dye in aqueous solution. The decolorization of the MG dye was examined under three different conditions (treatments): under UV and visible light irradiation without any catalyst (blank solution), in the presence of catalyst without light irradiation (in dark) and in the presence of $MnO_2/Al_2O_3/Fe_2O_3$ photocatalyst under UV and visible light irradiation, respectively. For the blank experiment (in the absence of the catalyst) under UV and visible light irradiation, almost insignificant degradation of the dye was observed (with only 3.4 and 4.2% decolorization efficiencies of the photocatalyst under visible and UV light irradiations, respectively). The percent adsorption values of MG dye is a function of time without the catalyst under visible and UV light irradiations. The corresponding plots of percent degradation as a function of time (under both visible and UV light irradiation) are shown in Figure 8.

In the presence of photocatalyst ($MnO_2/Al_2O_3/Fe_2O_3$), but without irradiation, only 6.98% decolorization efficiency was observed throughout the 180 min. This result confirms that degradation of the MG in the presence of the photocatalyst, but without light irradiation is insignificant. The fact is that no electron-hole pair could be generated in the semiconducting material without assistance of light irradiation (photoinduction). The formation of electrons and holes are responsible for enhancing the oxidation and reduction reactions with the malachite green dye, which might be adsorbed on the surface of the semiconductor to give the necessary products. Actually, the experimental results show that when the dye solution is exposed to UV and visible light irradiation for 180 min in the presence of $MnO_2/Al_2O_3/Fe_2O_3$ photocatalyst, about 69.30 and 92.89% of the MG dye could be degraded by UV and visible light irradiations, respectively. Accordingly, the degradation efficiency of MG dye under the visible light was found to be much larger than it was under the UV light irradiation. This enhancement under visible light in the presence of $MnO_2/Al_2O_3/Fe_2O_3$ photocatalyst could be explained from two reasons. The first one could be the fact that the $MnO_2/Al_2O_3/Fe_2O_3$ photocatalyst prepared by the sol gel method has a high specific surface area, that could give more active surface sites to adsorb water molecules and to form active •OH and HOO• radicals by trapping the photogenerated holes. This free active radical drive the photodegradation reactions and eventually leads to the decomposition of organic pollutants in aqueous solution (Bharathi et al., 2010).

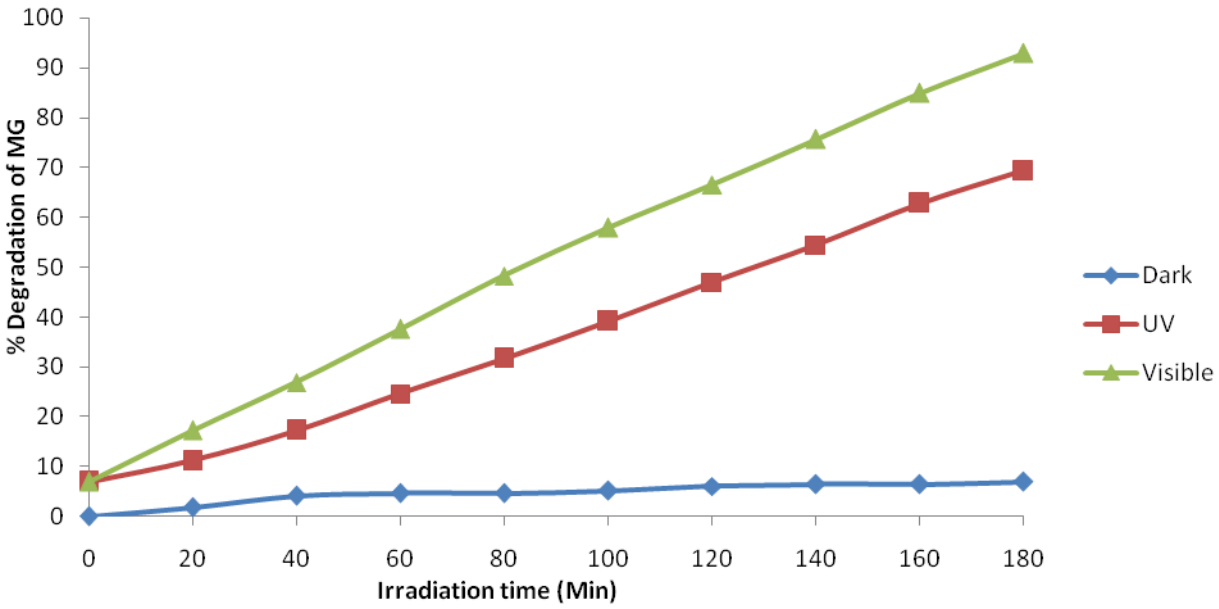

Figure 9. Plots of percentage degradation of malachite green dye as function of time (under UV, Visible and without irradiation) using $MnO_2/Al_2O_3/Fe_2O_3$ photocatalyst.

The higher surface area also facilitates the absorption of dye molecules on the surfaces of $MnO_2/Al_2O_3/Fe_2O_3$ photocatalyst. Under visible light irradiation, MG molecules are absorbed on the surfaces of nanocomposite and produced electrons. These electrons are captured by the surface adsorbed O_2 molecules to yield O_2•− and HO_2• radicals, which makes more chance to touch with dye molecules and giving a faster reaction speed then, the MG molecules could be mineralized in time by the super oxide radical ions. Therefore, it can be concluded that the smaller crystalline size of nanocomposite are favorable for the reduction of O_2 and oxidation of H_2O molecules by trapping electrons and holes, which improves the photocatalytic activity of the nanocomposites photocatalyst under visible light region.

The second reason could be the presumption that some of the Al (III) ions and Mn (IV) ions in the photocatalyst might be substituted by Fe (III) lattice site to form a stable solid solution. Such replacements of Al (III) and Mn (IV) ions by the Fe (III) ions can obviously create a charge imbalance (Ali Ismail, 2005). The charge imbalance must be satiated as Mn (IV) ions were reduced to Mn (III) ions. The existence of the Mn (IV) ions can thus inhibit the recombination of the photogenerated electron-hole pairs.

As a result, more OH^- ions would be adsorbed on the surface of the catalyst to overcome the charge balance. These OH^- ions present on the surface of the photocatalyst would accept the holes that are generated by the visible light illumination and thus converted to hydroxyl radicals (•OH), the radicals so formed can oxidize very easily the MG dye solution. On the other hand, the same visible light irradiation could be able to create oxygen vacancies on the structure of the photocatalyst structure. The oxygen vacancies formed as such can trap the electrons that are excited from the VB to the CB and thereby converted into superoxide radicals ($O•_2^-$) (Zhang et al., 2009). These $O^{\bullet}{}_2^-$ radicals are active enough to promote the oxidation of organic substances and effectively inhibited the electron-hole pair recombination. Therefore, these results show that the composite nanomaterial has a good photocatalytic performance in the degradation of MG dye in aqueous solution under visible light irradiation. The photodegradation values of MG dye as a function of time under UV and Visible light irradiations and without light irradiation are presented. Plot of percentage degradation as a function of time under UV, Visible and without irradiation are also shown in Figure 9.

Kinetic studies of photocatalytic degradation of MG

The adsorption of MG under without irradiation and its photocatalytic degradation under UV and Visible irradiations follow the pseudo first- order reaction kinetics expressed by the equation:

$$kt = \ln \frac{C_o}{C_t}$$

Where k is the reaction rate constant, C_0 is the initial concentration of MG solution and C_t is the concentration of MG solution at the reaction time t. The linear plot of $\ln C_o/C_t$ versus irradiation time *t* is shown in Figure 10 and values of rate constant (k) as a function of time is

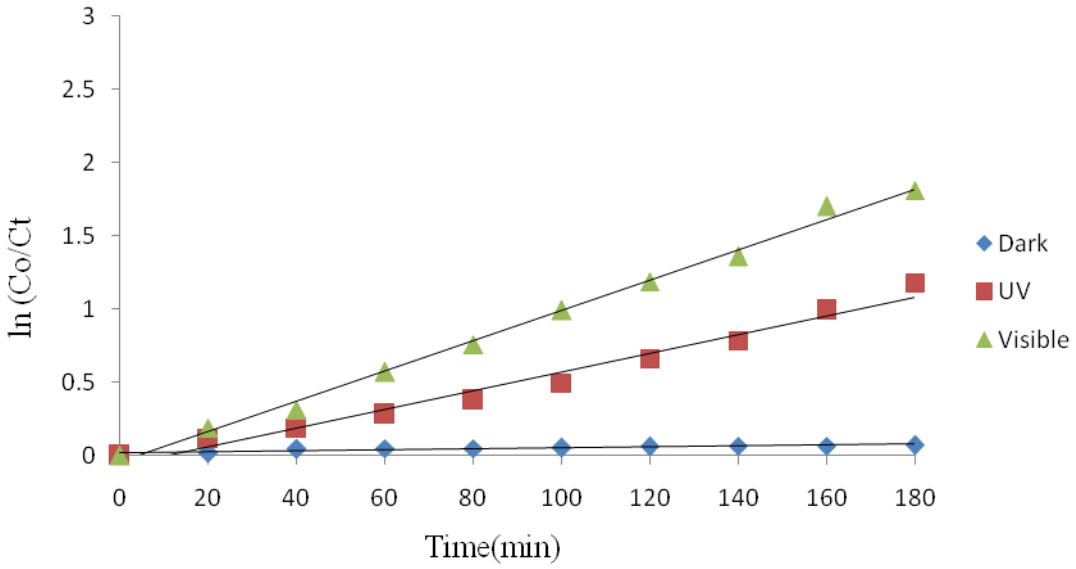

Figure 10. Plots of ln (C_0/C_t) vs. time for adsorption and photocatalytic degradation of MG in the presence of catalyst without irradiation, and under UV and Visible light irradiations.

Table 5. ln (C_0/C_t) as a function of time without irradiation, and under UV and Visible light irradiations in the presence of the photocatalysts.

Time(min)	ln(C_0/C_t) in Dark	ln(C_0/C_t) under UV	ln(C_0/C_t) under Visible
0	0.000	0.000	0.000
20	0.019	0.118	0.189
40	0.043	0.189	0.313
60	0.048	0.283	0.571
80	0.048	0.380	0.758
100	0.053	0.495	0.994
120	0.062	0.663	1.190
140	0.067	0.786	1.360
160	0.067	0.989	1.700
180	0.072	1.180	1.810

presented in Table 5. The calculated adsorption rate constant for MG using $MnO_2/Al_2O_3/Fe_2O_3$ photocatalyst without irradiation is 4×10^{-4} min^{-1}. The calculated rate constants for the degradation of this dye under the UV and visible light irradiations using the same catalyst were found to be 6.56×10^{-3} and 1.0×10^{-2} min^{-1}, respectively. Determination coefficients (R^2) of the pseudo-first order reaction without light irradiation, under UV and visible light irradiations were found to be 0.856, 0.976 and 0.995, respectively.

Comparison of binary and ternary photocatalytic activities

In order to explore the photocatalytic activity of the binary and ternary mixed oxides, various studies had been carried out to search ideal semiconductor photocatalyst for degradation of organic pollutants. The result is shown in Table 6. It can be seen that the photocatalytic activities of the ternary mixed oxide photocatalyst displays significantly high degradation ability for organic pollutants in aqueous solution. The improvement may be explained in terms of synergetic effect on the specific adsorption property and the efficient electron-hole separation at the coupled ternary mixed oxides photocatalyst interface. However, up till now no $MnO_2/Al_2O_3/Fe_2O_3$ coupled ternary photocatalyst has been reported for degradation of organic pollutants. These nanocomposite photocatalyst were found to be more photoeffective than binary Al_2O_3/Fe_2O_3 photocatalyst for oxidation of organic compound.

Table 6. Comparison of the photodegradation efficiency of organic dye in term of binary and ternary photocatalyst

Binary photocatalysts	Types of dye	Degradation efficiency (%)	Ternary photocatalysts	Types of dye	Degradation efficiency (%)
ZnO/Cu_2O	MO	73	$TiO_2{\cdot}[ZnFe_2O_4]_x$	Congo Red	90
Al_2O_3/Fe_2O_3	Bisphenal A	60	$Y_2O_3/Fe_2O_3/TiO_2$	EDTA	92
Fe_2O_3/TiO_2	MO	85	Fe_2BiSbO_7	MB	96.59
Al_2O_3/CeO_2	Congo red	80	Sr_2FeMoO_6	Acid Red B	100
$Al/Al_2O_3/TiO_2$	Cypermethrin	60.4	Ag/S/ZnO	MG	98
MnO_2/ZnO	MB	50	-	-	-

SUMMARY AND CONCLUSIONS

New composite nanosized $MnO_2/Al_2O_3/Fe_2O_3$ photocatalyst with a rhombohedral structure and oxygen vacancies was successfully synthesized by the sol-gel method by using metal salts as a starting materials. The as-synthesized materials were characterized by AAS, XRD, FTIR and UV/Visible spectroscopic techniques. The XRD pattern suggested that the as-synthesized nanopowders have a crystal structure with a good nonosized range of 20 to 26 nm particle sizes. Smallest particle size of catalyst was taken for characterization and photodegradation study of MG dye. Its band gap energy was about 1.97 eV, which is an important band gap for improving photocatalytic degradation of organic dyes in the visible region. The FTIR spectra before and after calcination are shown as -OH and Fe-O vibration bond in the as-synthesized photocatalyst calcinied at 400°C. Photocatalytic degradation of malachite green in aqueous solution was carried out under different conditions. It was included in the absence of the catalyst, under both UV and visible light irradiations (in blank), without light irradiation (in dark), and under both UV and visible light irradiations in the presence of the photocatalyst. The experimental results showed that higher decolorization efficiency was obtained under visible light irradiation in the presence of the catalyst. This may be due to the larger specific surface area, formation of oxygen vacancies and mixed valence states of manganese in the structure of the $MnO_2/Al_2O_3/Fe_2O_3$ photocatalyst.

Conflict of Interests

The authors have not declared any conflict of interests.

REFERENCES

Ali Ismail A (2005). Synthesis and characterization of $Y_2O_3/Fe_2O_3/TiO_2$ nanoparticles by sol–gel method. App. Cat. B: Environ. 58:115-121.

Baldrian P, Merhautova V, Gabriel J, Nerud F, Stopka P, Hruby M (2006). Decolorization of synthetic dyes by hydrogen peroxide with heterogeneous catalysis by mixed iron oxides. App. Cat. B: Env. 66:258-264.

Bharathi S, Nataraj D, Mangalaraj D, Masuda Y, Senthil K , Yong K (2010). Highly mesoporous α-Fe_2O_3 nanostructures: preparation, characterization and improved photocatalytic performance towards Rhodamine B (RhB). J. appl. Phy.43:015501 9p.

Brijesh P, Pardeep S, Jonnalagadda SB (2008). Visible light induce heterogeneous advancedoxidation process to degrade pararosanilin dye in aqueous suspension ZnO. Int. J. Chem. 47:830-835.

Chien-Tsung W (2007). Photocatalytic activity of nanoparticle gold/iron oxideaerogels for azo dye degradation. J. Non-Cry. Solids. 353:1126-1133.

Chu X, Zhang H (2009). Catalytic Decomposition of Formaldehyde on Nanometer manganese Dioxide. Mod. Appl. Sci. 3(4).

Cordier A, Peigney A, Grave ED, Flahaut E, Laurent C (2006). Synthesis of the metastable α-$Al_{1.8}Fe_{0.2}O_3$ solid solution from precursors prepared by combustion. J. Eur. Ceram. Soc. 26:3099-3111.

El-Moselhy MM (2009). Photo-degradation of acid red 44 using Al and Fe modified silicates. J. Hazard. Mater.169:498-508.

Gomathi DL, Murthya BN,Kumar SG (2009). Heterogeneous photo catalytic degradation of anionic and cationic dyes over TiO_2 and TiO_2 doped with Mo^{6+} ions under solar light:Correlation of dye structure and its adsorptive tendency on the degradation rate. Chem. 76:1163-1166.

Jia-feng W, Hai-tao W, Peng-yu Z, Ming-jing G (2011). Catalytic oxidation degradation of phenol in wastewater by heterogeneous Fenton reagent. J. Chong. University (English Edition) 10(4):1671-8224.

Kang M, Park ED, Kim JM, Yie JE (2007). Manganese oxide catalysts for NOx reduction with NH3 at low temperatures. Appl. Cats. A: Gen. 327:261-269.

Karakassides AM and Gournis D (2003). Magnetic Fe_2O_3–Al_2O_3 composites prepared by a modified wet impregnation method. J.Mater.chem. 13:871-876.

Kitis M, Kaplan SS 2007. Advanced oxidation of natural organic matter using hydrogen peroxide and iron-coated pumiceparticles. Chemical 68:1846-1853.

Laat JD, Le TG (2006). Effects of chloride ions on the iron (III)-catalyzed decomposition of hydrogen peroxide and on the efficiency of the Fenton-like oxidation process. Appl. Catal. B: Envion. 66:137-146.

Lei J, Liu C, Li F, Li X, Zhou S, Liu T, Gu M, Wu Q (2006). Photodegradation of orange I in the heterogeneous iron oxide–oxalate complex system under UVA irradiation. J. Hazard. Mater. B. 137:1016-1024.

Leland JK, Bard AJ (1987). Photochemistry of colloidal semiconducting iron oxide polymorphs. J. Phys. Chem. 91:5076-5083.

Li C, Zhang HJ, Chen ZQ (2010). Chemical quenching of positronium in Fe_2O_3/Al_2O_3 catalysts. Appl. Surf. Sci. 256:6801-6804.

Li FB, Li XZ, Liu CS,Liu TX (2007). Effect of alumina on photocatalytic activity of iron oxides for bisphenol degradation. J. Hazard. Mater. 149:199-207.

Mitta N, Shah A, Punjabi PB,Sharma VK (2009). Photodegradation Of Rose Bengal Using MnO_2 (Manganese Dioxide). Rasayan J. Chem. 2(2):516-520.

Neiva LS, Andrade MC, Costa CFM, Gama L (2009). Synthesis Gas (Syngas) production over Ni/Al_2O_3 catalysts modified with Fe_2O_3.

Braz. J. Petr.Gas. 3(3):083-091.
Park J, Lee Y, Khanna PK, Juna K, Bae JW,Kim YH (2010). Alumina-supported iron oxide nanoparticles as Fischer–Tropsch catalysts: Effect of particle size of iron oxide. J. Mol. Catal. A Chem.323:84-90.
Pattanayak CB (2010). Synthesis and Characterization of Alumina/Iron Oxide Mixed Nanocomposite. N. Int. Technol. Rourkela Rourkela 769008.
Rhoton FE, Bigham JM,Lindbo DL (2002). Properties of iron oxides in streams draining the Loess Uplands of Mississippi. Appl. Geochem. 17:409-419.
Sakthivel S, Shankar MV, Palanichamy M, Arabindoo B, Bahnemann DW,Urugesan V (2005). Enhancement of photocatalytic activity by metal depoitions: Characterisatsion and photonic efficiency of Pt, Au and Pd depoited on TiO_2 catalyts. Water Res. 38:3001-3008.
Su P (2010). Studies on Catalytic Activity of Nanostructure Mn_2O_3 Prepared by Solvent-thermal Method on Degrading Crystal Violet. Mod. Appl. Sci. 4(5).
Torres-Martinez LM, Juarez-Ramirez I, Ramos-Garza JS, Azquez-Acosta FV, Lee SW (2010). Bi_2MTaO_7 (M = Al, Fe, Ga, In) Photocatalyst for Organic Compounds Degradation under UV and Visible Light. WSEAS Trans. Environ. Dev.4(6).
Wang YC, Liua S, Li FB, Liu CP, Liang JB (2009). Photodegradation of polycyclic aromatic hydrocarbon pyrene by iron oxide in solid phase. J. Hazard. Mater.162:716-723.
Yan H, Pan W, An-Ping D, Jing Y, Ying-Ping H, Yong Y (2010). Preparation of CdS Nanoparticles with Reverse Micelle Method and Photo-degradation of malachite Green Dye. J. Ino. Mat. 25(11).
Zelmanov G, Semiat R (2008). Iron(3) oxide-based nanoparticles as catalysts in advanced organic aqueous oxidation. Water Res. 42:492-498.
Zhang G, Yang J, Zhang S, Xiong Q, Huang B, Wang J ,Gong W (2009). Preparation of nanosized Bi_3NbO_7 and its visible-light photocatalytic property. J. Hazard. Mater.172:986-992.
Zhao S, Wu HY, Song L, Tegus O, Asuha S (2009). Preparation of *c*-Fe_2O_3 nanopowders by direct thermal decomposition of Fe-urea complex: reaction mechanism and magnetic properties. J. Mater. Sci.44:926-930.

African Journal of Pure and Applied Chemistry

Related Journals Published by Academic Journals

- *African Journal of Mathematics and Computer Science Research*
- *International Journal of the Physical Sciences*
- *Journal of Geology and Mining Research Technology*
- *Journal of Environmental Chemistry and Ecotoxicology*
- *Journal of Internet and Information Systems*
- *Journal of Oceanography and Marine Science*
- *Journal of Petroleum Technology and Alternative Fuels*

academicJournals